Atmos. Meas. Tech., 8, 5099–5112, 2015
www.atmos-meas-tech.net/8/5099/2015/
doi:10.5194/amt-8-5099-2015

Atmospheric Measurement Techniques
Open Access
EGU

Can AERONET data be used to accurately model the monochromatic beam and circumsolar irradiances under cloud-free conditions in desert environment?

Y. Eissa[1,2], P. Blanc[1], L. Wald[1], and H. Ghedira[2]

[1]MINES ParisTech, PSL Research University, O.I.E., Centre Observation, Impacts, Energy, CS 10207, 06904 Sophia Antipolis CEDEX, France
[2]Masdar Institute, Research Center for Renewable Energy Mapping and Assessment, Abu Dhabi, P.O. Box 54224, UAE

Correspondence to: Y. Eissa (yeissa@masdar.ac.ae)

Received: 17 June 2015 – Published in Atmos. Meas. Tech. Discuss.: 24 July 2015
Revised: 18 November 2015 – Accepted: 23 November 2015 – Published: 8 December 2015

Abstract. Routine measurements of the beam irradiance at normal incidence include the irradiance originating from within the extent of the solar disc only (DNI_S), whose angular extent is $0.266° \pm 1.7\,\%$, and from a larger circumsolar region, called the circumsolar normal irradiance (CSNI). This study investigates whether the spectral aerosol optical properties of the AERONET stations are sufficient for an accurate modelling of the monochromatic DNI_S and CSNI under cloud-free conditions in a desert environment. The data from an AERONET station in Abu Dhabi, United Arab Emirates, and the collocated Sun and Aureole Measurement instrument which offers reference measurements of the monochromatic profile of solar radiance were exploited. Using the AERONET data both the radiative transfer models libRadtran and SMARTS offer an accurate estimate of the monochromatic DNI_S, with a relative root mean square error (RMSE) of 6 % and a coefficient of determination greater than 0.96. The observed relative bias obtained with libRadtran is $+2\,\%$, while that obtained with SMARTS is $-1\,\%$. After testing two configurations in SMARTS and three in libRadtran for modelling the monochromatic CSNI, libRadtran exhibits the most accurate results when the AERONET aerosol phase function is presented as a two-term Henyey–Greenstein phase function. In this case libRadtran exhibited a relative RMSE and a bias of respectively 27 and $-24\,\%$ and a coefficient of determination of 0.882. Therefore, AERONET data may very well be used to model the monochromatic DNI_S and the monochromatic CSNI. The results are promising and pave the way towards reporting the contribution of the broadband circumsolar irradiance to standard measurements of the beam irradiance.

1 Introduction

The direct, or beam, normal irradiance (DNI) is the radiant flux per unit area received on a plane normal to the Sun rays from a small solid angle centred to the solar disc (ISO-9488, 1999; WMO, 2010). The DNI plays a role in various domains, such as natural biomass development, climate, daylighting or concentrated solar technologies (CST) in electricity production. In the ISO definition of the DNI the "small solid angle" is not defined. In modern instruments the aperture (or opening) half-angles range between 2.5 and 5°, respectively equivalent to solid angle apertures of 6 msr and 24 msr. The World Meteorological Organization (WMO) recommends that all new designs of DNI measuring instruments to have an aperture half-angle of 2.5° (WMO, 2010).

For an observer at the surface of the Earth, the Sun has an angular radius of $0.266° \pm 1.7\,\%$ (Jilinski et al., 1998). CST systems have aperture half-angles larger than the angular radius of the solar disc but usually smaller than those of the measuring instruments (Blanc et al., 2014). This implies that the irradiance originating from within the extent of the solar disc only (DNI_S) and that from a larger circumsolar region defined by the solid angle aperture, called the circumsolar normal irradiance (CSNI), are intercepted within the aperture

of the measuring instrument or concentrating system. This paper deals with the modelling of the DNI_S and CSNI.

To tackle the ambiguity of the "small solid angle", Blanc et al. (2014) recommend reporting the viewing angles of the measuring instrument along with the sunshape and contribution of the circumsolar irradiance in addition to the DNI measured by pyrheliometers or equivalent pyranometric systems. The contribution of the CSNI may be provided in terms of CSNI defined for the solid angle aperture, or in terms of the circumsolar ratio (CSR), which is the ratio of the CSNI to the sum of the CSNI and DNI_S (Buie et al., 2003). The sunshape is the azimuthally averaged profile of solar radiance normalized with respect the central, i.e. maximum, radiance reading. The solar radiance profile represents the angular distribution of the sky radiance from which the CSNI is computed.

Reporting the sunshape and the contribution of circumsolar radiation are not straightforward when no coinciding measurements of such are available. Several ground measurement campaigns of the solar radiance profile have taken place, but the data sets are limited in space and time (Neumann et al., 2002; Noring et al., 1991). More recent and still ongoing campaigns have measured or are still measuring the monochromatic profile of solar radiance at a resolution of $\sim 0.015°$ up to an angular distance of $\sim 8°$ from the centre of the solar disc with the Sun and Aureole Measurement (SAM) instrument. SAM only measures the monochromatic radiance at 670 nm with a full spectral width at half-maximum of 10 nm. Other spectral filters exist at 440 and 870 nm. This instrument is manufactured by Visidyne Inc., and the data are available for public access (http://www.visidyne.com/). Out of the nine instruments reported on the website, six of them have data available for download for three instruments located in France, Spain and the United Arab Emirates (UAE) and three in the USA.

Wilbert (2014) and Wilbert et al. (2013) propose a method to convert the SAM monochromatic measurements of the profile of solar radiance to broadband profiles using a modified version of the radiative transfer model (RTM) SMARTS (Simple Model of the Atmospheric Radiative Transfer of Sunshine; Gueymard, 1995, 2001). Reinhardt (2013) and Reinhardt et al. (2014) use cirrus cloud properties derived from Meteosat satellite imagery to estimate the broadband circumsolar radiation by the use of look-up tables established with the Monte Carlo radiative transfer solver available in libRadtran (Mayer and Kylling, 2005; Mayer et al., 2012). Other preliminary works (Eissa et al., 2014; Oumbe et al., 2012) have modelled the broadband CSNI, but the results have not been compared with reference measurements.

AERONET (Aerosol Robotic Network) products provide the aerosol optical properties at numerous locations globally and for varying time periods (Holben et al., 1998). Masdar City, located in the suburbs of Abu Dhabi, UAE, is the seat of both AERONET and SAM measurements. It offers the opportunity to study the potentials of AERONET data in modelling the DNI_S and CSNI.

The objective of this article is to answer the following question: can AERONET data be used to accurately model the monochromatic beam and circumsolar irradiances under cloud-free conditions in desert environment? A desert environment is of interest because countries in the Middle East and North Africa region, where the environment is mostly dominated by desert surroundings, have set ambitious plans to install CST systems in the upcoming years (Brand and Zingerle, 2011; Griffiths, 2013). In desert environments the circumsolar radiation may be significant under turbid cloud-free skies, implying that information of the CSNI and DNI_S is essential for an improved assessment of the DNI (Blanc et al., 2014). For example, Thomalla et al. (1983) report a CSR of 0.06 for an aperture half-angle of 5° when using a desert aerosol model for a solar zenith angle of 70° and an aerosol optical depth (AOD) at 550 nm of 0.4.

To that extent, several parameterizations of the monochromatic phase function, asymmetry parameter and single scattering albedo available in the RTMs libRadtran and SMARTS are tested against SAM measurements, where the aerosol optical properties are extracted from the products of AERONET.

The article is organized as follows: theoretical background (Sect. 2), aerosol optical properties from AERONET data (Sect. 3), SAM data (Sect. 4), cross-comparison between AERONET and SAM data (Sect. 5), AERONET data in the parameterizations of the RTMs (Sect. 6), results and discussion (Sect. 7) and conclusions (Sect. 8).

2 Theoretical background

2.1 The beam irradiance

In radiative transfer modelling, the monochromatic DNI_S only comprises photons that were not scattered and is represented by the Beer–Bouguer–Lambert law (Liou, 2002) as

$$B_{n,\lambda}^{\text{strict}} = E_{0,n,\lambda} \exp(-\tau_\lambda m), \quad (1)$$

where $B_{n,\lambda}^{\text{strict}}$ is the monochromatic DNI_S from radiative transfer modelling point of view, $E_{0,n,\lambda}$ is the monochromatic extraterrestrial irradiance received on a plane normal to the Sun rays, τ_λ is the monochromatic optical depth of all attenuating factors present in the atmosphere and m is the pressure-corrected relative optical air mass (Kasten and Young, 1989). Therefore, accurate modelling of $B_{n,\lambda}^{\text{strict}}$ requests an accurate retrieval of τ_λ within the extent of the solar disc only.

For ground measurements of the monochromatic DNI_S it is not possible to distinguish whether a photon was scattered or not before reaching the measuring instrument (Blanc et al., 2014). Therefore, in this work it is assumed that the effects of scattered photons within the extent of the solar disc are negligible, and $B_{n,\lambda}^{\text{strict}}$ is validated against the ground reference monochromatic DNI_S, noted $B_{n,\lambda}^{\text{Sun}}$. To this end,

the monochromatic DNI_S modelled by the radiative transfer codes is also noted $B^{Sun}_{n,\lambda}$. The ground reference monochromatic DNI_S may be computed from measurements of the beam radiance within the solar disc as (Blanc et al., 2014; Buie et al., 2003)

$$B^{Sun}_{n,\lambda} = \int_0^{2\pi}\int_0^{\delta_S} L_\lambda(\xi,\phi_n)\cos(\xi)\sin(\xi)\mathrm{d}\xi\,\mathrm{d}\phi_n, \quad (2)$$

where $L_\lambda(\xi, \varphi_n)$ is the monochromatic beam radiance, ξ is the angular distance from the centre of the Sun, φ_n is the azimuth angle on the plane normal to the solar beam direction and δ_S is the angular radius of the Sun corrected with respect to the Sun–Earth distance. For the small ξ of the solar and circumsolar regions the deviation from 1 of the $\cos(\xi)$ term can be considered negligible, and $\sin(\xi) \approx \xi$. Also, under the assumption of radial symmetry of the sky radiance in the vicinity of the Sun under cloud-free conditions, Eq. (2) simplifies to

$$B^{Sun}_{n,\lambda} \approx 2\pi \int_0^{\delta_S} L_\lambda(\xi)\xi\mathrm{d}\xi. \quad (3)$$

2.2 The circumsolar irradiance

The CSNI is computed from the circumsolar diffuse radiance as (Blanc et al., 2014; Buie et al., 2003)

$$CS_{n,\lambda}(\delta,\alpha) \approx 2\pi \int_\delta^\alpha L_\lambda(\xi)\sin(\xi)\mathrm{d}\xi \approx 2\pi \int_\delta^\alpha L_\lambda(\xi)\xi\mathrm{d}\xi, \quad (4)$$

where $CS_{n,\lambda}(\delta, \alpha)$ is the monochromatic CSNI in the interval $[\delta, \alpha]$, δ is the inner limit of the circumsolar region, α is the outer limit of the circumsolar region and $L_\lambda(\xi)$ is monochromatic diffuse radiance.

The monochromatic diffuse radiance is a function of the monochromatic optical depth, the monochromatic single scattering albedo and the monochromatic phase function (Dubovik and King, 2000).

3 Aerosol optical properties from AERONET data

The environment of interest is that of Masdar City, located in the suburbs of Abu Dhabi, UAE. The site is described as near-coastal, desert and urban, with frequent cloud-free but turbid skies due to natural and anthropogenic dust emissions (Gherboudj and Ghedira, 2014). It has an altitude above mean sea level of 2 m and is located at 24° 26′ 30.58″ N, 54° 36′ 59.75″ E. Coinciding AERONET and SAM measurements were performed from June 2012 to May 2013, the instruments are ∼ 55 m apart and measurements are still ongoing.

The CIMEL CE-318 Sun photometer of the AERONET station has an aperture half-angle of 0.6° (Holben et al., 1998). The monochromatic vertical column AODs, noted $\tau_{a,\lambda}$, are provided at the following wavelengths: 1640, 1020, 870, 675, 500, 440, 380 and 340 nm, from the Version 2 Direct Sun Algorithm (DSA) products. The AODs for wavelengths greater than 440 nm have a reported uncertainty of ±0.01 (Eck et al., 1999). The total column content in water vapour, with an uncertainty of ∼ 10 % (Holben et al., 2001), and the solar zenith angle θ_S are also reported. In this work, only Level 2.0 DSA products were used to ensure cloud-free and quality-assured observations. The cloud-screening algorithm of the AERONET data only filters out the cloud-contaminated observations in the direction of the Sun (Smirnov et al., 2000).

Version 2 inversion products are also available from the AERONET data. They include the monochromatic radiance measurements as a function of azimuth deviations from the solar azimuth angle in the almucantar plane, measured at the following wavelengths: 1020, 870, 675 and 440 nm. In the near vicinity of the solar disc the almucantar measurements of radiance are provided over Masdar City at azimuth angular deviations of ±3, ±3.5, ±4, ±5 and ±6°. The AERONET sky radiance measurements have a reported uncertainty < 5 % primarily due to calibration uncertainty (Holben et al., 1998).

From June 2012 to May 2013 there are 2241 profiles of the diffuse radiance notably at 675 nm in the almucantar plane, all in Level 2.0. The wavelength of 675 nm is of specific interest in this study because it almost coincides with the radiance measurements of the SAM instrument, discussed in Sect. 4.

The AERONET Version 2 inversion products also include (Dubovik and King, 2000; Dubovik et al., 2002, 2006; Holben et al., 1998)

- the monochromatic aerosol single scattering albedo, noted $\omega_{a,\lambda}$;
- the monochromatic aerosol phase function provided at 83 scattering angles, where the scattering angle is approximated by ξ (Wilbert et al., 2013), noted $P_{a,\lambda}(\xi)$;
- the monochromatic asymmetry parameter, noted g_λ.

For this time period, and in Level 2.0, there are 1068 observations of $\tau_{a,\lambda}$, $P_{a,\lambda}(\xi)$ and g_λ covering the whole 12 months of this study period. The months with the smallest number of observations are November and December 2012 and May 2013, with respectively 4, 5 and 4 % of the 1068 observations. For the remaining months the number of observations ranges between 8 and 14 % of the 1068 observations. Only 491 from the 1068 observations include $\omega_{a,\lambda}$, because $\tau_{a,440\,nm}$ must be greater than 0.4 to achieve useful accuracy in $\omega_{a,\lambda}$. The distribution of the 491 samples amongst the months varies widely. There are two samples in November 2012. October and December 2012 and January, February, March and May 2013 offer a small number of samples,

smaller than 26. The 5 remaining months offer larger numbers of samples.

Table 1 presents the mean, minimum, maximum and standard deviation of $\tau_{a,675\,\mathrm{nm}}$, $\omega_{a,675\,\mathrm{nm}}$ and $P_{a,675\,\mathrm{nm}}(\xi)$ for both the 1068 samples (excluding $\omega_{a,675\,\mathrm{nm}}$) and the 491 samples. These statistics are presented for $P_{a,675\,\mathrm{nm}}(\xi)$ for the three ξ smaller than 6° reported in the AERONET Version 2 inversion products, i.e. 0, 1.71 and 3.93°.

The relative standard deviation of $\tau_{a,675\,\mathrm{nm}}$ for the 1068 samples is very large at 69 % of the mean value, indicating its great temporal variability and its significance in modelling both the monochromatic $\mathrm{DNI_S}$ and diffuse radiance. The relative standard deviation of $P_{a,675\,\mathrm{nm}}(\xi)$ is also large, ranging between 18 and 24 % for the three smallest ξ for the 1068 samples, again implying its significance in modelling the diffuse radiance.

On the contrary, the relative standard deviation of $\omega_{a,675\,\mathrm{nm}}$ is small at 0.019 (2 % of the mean value) for the 491 samples. The uncertainty of the AERONET $\omega_{a,675\,\mathrm{nm}}$ retrievals is not provided, it is reported at $\omega_{a,440\,\mathrm{nm}}$ and is 0.03 (Dubovik et al., 2000). When the multiple scattering effects are ignored, the diffuse radiance is linearly proportional to the single scattering albedo (Dubovik and King, 2000; Liou, 2002; Wilbert et al., 2013). A practical consequence is that a mean value of $\omega_{a,675\,\mathrm{nm}}$ can be used with an acceptable loss of accuracy. In addition, using a mean value of $\omega_{a,\lambda}$ is a means to tackle the issue of the missing $\omega_{a,\lambda}$ values at instances when $P_{a,\lambda}(\xi)$ data are available. The AERONET retrievals of $\omega_{a,\lambda}$ are not provided under small aerosol loading situations and this causes the gaps in $\omega_{a,\lambda}$ (Dubovik et al., 2000; Yin et al., 2015).

The mean value of $\omega_{a,675\,\mathrm{nm}}$ for the available 491 observations over this study area and for this study period is 0.954, this number is fairly close to the monthly mean values of $\omega_{a,675\,\mathrm{nm}}$, which range from a minimum of 0.917 in December 2012 to a maximum of 0.974 reached in March 2013. In the extreme case of the minimum observed value (0.881), an error of 8 % will be induced on the diffuse radiance by opting to use a mean value of $\omega_{a,675\,\mathrm{nm}}$. However, this is a rare situation. Indeed, 67 % of the $\omega_{a,675\,\mathrm{nm}}$ samples lie within the mean ± 1 standard deviation and 96 % lie within the mean ± 2 standard deviations. For the 491 samples, the mean error in the diffuse radiance incurred by assuming an average value of $\omega_{a,675\,\mathrm{nm}}$ is < 2 %.

4 SAM data

The ground measurements of the beam and circumsolar diffuse radiance were collected at Masdar City by the SAM instrument (DeVore et al., 2012a, b). The instrument is located at 24° 26′ 32.36″ N, 54° 36′ 59.60″ E. The instrument is comprised of two cameras (Wilbert et al., 2013). One directly measures the radiance within the solar disc. The solar aureole, also known as the circumsolar region, is formed on a screen with a beam dump for the solar disc region and this image is captured by the other camera facing the screen. The monochromatic radiance at Masdar City is measured only at 670 nm with a full spectral width at half-maximum of 10 nm. The angular resolution of the radiance measurements is 0.0217° and the acquisition frequency is 4 or 5 times per minute. The relative error of the beam radiance is reported to be less than 1 % for $\tau_{a,670\,\mathrm{nm}} < 0.6$, while that of the aureole radiance is reported to be between 5 and 15 % (Stair and DeVore, 2012). An angular gap exists between the beam and circumsolar radiance measurements to avoid superimposition of the solar disc radiance scattered on the screen with the image of the circumsolar region on that screen (Wilbert et al., 2013). For the SAM 400 series, as the one in Masdar City, measurements from the aureole camera for $\xi < 0.52$ are discarded (Wilbert, 2014). The internal scattering correction of DeVore et al. (2012b) was not applied to the downloaded SAM data.

There are four main files of SAM data for each day (LePage et al., 2008). One file comprises the horizontal, and another the vertical, beam and circumsolar radiance measurements. One file contains the azimuthally averaged profiles of solar radiance. The reported angular resolution for all radiance data is 0.0217°. The last file includes the particulate optical depth at 670 nm and θ_S. In this study the matching of AERONET and SAM data is only performed under cloud-free conditions; hence the particulate optical depth is basically $\tau_{a,670\,\mathrm{nm}}$.

The SAM instrument is fairly new. The oldest reference found was that of DeVore et al. (2007), who reported examples of the SAM measurements collected in 2006. However, no article has been found which clearly defines quality-control procedures for the SAM measurements. There are also several gaps in the downloaded data. A series of tests have been applied herein to retain only the high-quality measurements and possibly remove cloud-contaminated ones.

i. The number of profiles of solar radiance and $\tau_{a,670\,\mathrm{nm}}$ observations do not match. Therefore, the radial, horizontal and vertical profiles were matched to the $\tau_{a,670\,\mathrm{nm}}$ observations which have the same time stamp. With this test 229 561 observations of the profiles and $\tau_{a,670\,\mathrm{nm}}$ remain from originally 244 609 profiles.

ii. Any radial profile with negative values in the solar disc region is removed; 222 742 observations remain.

iii. The monochromatic radiance of the radial profile should decrease with an increasing angular displacement in the solar disc region, i.e. the condition $\mathrm{d}L_\lambda(\xi)/\mathrm{d}\xi < 0$ must be fulfilled. This procedure is similar to that proposed by Buie et al. (2003) when performing the quality checks on the profiles of solar radiance measured by the Lawrence Berkeley National Laboratory. With this test 222 714 observations remain.

Table 1. Basic statistics of $\tau_{a,675\,\mathrm{nm}}$, $P_{a,675\,\mathrm{nm}}(\xi)$ and $\omega_{a,675\,\mathrm{nm}}$.

Variable	Sample no.	Mean	Minimum	Maximum	Standard deviation
$\tau_{a,675\,\mathrm{nm}}$	491	0.500	0.181	1.873	0.209 (42 %)
	1068	0.324	0.025	1.873	0.222 (69 %)
$P_{a,675\,\mathrm{nm}}(0°)$	491	179.6	73.7	322.6	31.9 (18 %)
	1068	173.9	64.7	412.7	41.4 (24 %)
$P_{a,675\,\mathrm{nm}}(1.71°)$	491	127.6	48.6	191.3	19.2 (15 %)
	1068	120.7	42.3	219.2	23.9 (20 %)
$P_{a,675\,\mathrm{nm}}(3.93°)$	491	62.7	21.7	80.4	8.9 (14 %)
	1068	58.7	21.4	80.5	10.4 (18 %)
$\omega_{a,675\,\mathrm{nm}}$	491	0.954	0.881	0.987	0.019 (2 %)
	1068	N/A	N/A	N/A	N/A

iv. According to Buie et al. (2003) and Neumann et al. (2002) the variations in the solar disc region of the sunshape are low for CSRs ranging between 0.05 and 0.4. When comparing the solar disc region of the CSR 0 and CSR 40 sunshapes proposed by Neumann et al. (2002) a relative root mean square error (RMSE) of 4 % is observed when taking the CSR 0 sunshape as the reference. The RMSE was constructed from the relative intensity of each sunshape at the different ξ. To this end, each SAM radiance measurement in the solar disc region was normalized between 0 and 1. In the solar disc region, a mean normalized solar radiance profile was generated from all the available measurements resulting from point (iii), which was then matched to the closest actual normalized profile in terms of Euclidean distance. Then the relative RMSE was computed for each normalized solar radiance profile with respect to the actual mean normalized profile. The 90th percentile of the RMSE was chosen as the cutoff. It also coincides with a relative RMSE of 4 %; 200 443 profiles pass this test.

v. As pointed out by Noring et al. (1991), the circumsolar radiance and ξ exhibit a linear relation in the log-log space. Therefore, the correlation coefficient in the log-log space was computed between the circumsolar radiance of each of the radial profiles and ξ in the interval [0.52°, 6°]. Any radial profile exhibiting a correlation coefficient less than 0.990 was eliminated; 188 801 observations remain.

5 Cross-comparison between AERONET and SAM data

Both SAM and AERONET data include L_λ and $\tau_{a,\lambda}$. A cross-comparison between them provides a confirmation on the reliability of the measurements of both instruments.

To compare the AERONET and SAM radiance measurements, the 2241 profiles of AERONET almucantar radiance measurements in the period June 2012 to May 2013 were matched to the SAM horizontal monochromatic radiance measurements which pass the procedures presented in Sect. 4 in terms of the time stamp. In the temporal matching process, the measurements between the two different instruments had to be at most 1 min apart and θ_S reported by the two instruments had to match: the bias between the matched θ_S was found to be 0.00° and the maximum absolute error in angle for all observations was 0.22°.

The corresponding ξ of the AERONET almucantar radiance measurements were computed from θ_S and the reported relative azimuth angles. The SAM radiance measurements were then angularly aggregated to match the 0.6° half field of view of the CIMEL 318 Sun photometer using the weighting method described in Wilbert (2014). After matching the measurements, 1067 AERONET and SAM profiles remained. The measurements with the same ξ to the east and west directions of the Sun were averaged to minimize the effects of small pointing errors (Torres et al., 2013). Ideally for these 1067 profiles there should be 5335 measurements of radiance corresponding to the five values from AERONET for $\xi < 6°$, where the maximum ξ from the AERONET measurements was found to be 5.8°. Instead there is a lower number of observations, 5236 to be exact, due to missing data in the almucantar measurements from AERONET which could occur at any ξ. The standard deviation of the differences between these remaining pairs of observations was computed. Then, all samples exhibiting a difference greater than three times this standard deviation were filtered out. This filter is meant to remove extreme cases which could occur if one instrument is shaded by clouds while the other is not. This situation can occur since the two instruments are not exactly at the same place, ~ 55 m apart, and the time matching is in minutes. Out of 5236, 133 pairs were excluded.

Figure 1 exhibits the density scatter plot (or 2-D histogram; Eilers and Goeman, 2004) of the SAM and AERONET radiance measurements. Red dots correspond to regions with high densities of samples and the dark blue ones to those with very low densities of samples. The relative RMSE is 14 %, the relative bias is 0 % and the coefficient of determination R^2 is high at 0.933. The observations are well scattered around the 1 : 1 line. The comparison re-

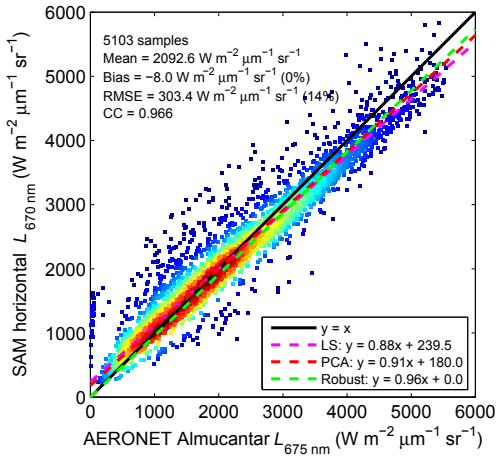

Figure 1. Scatter density plot between the SAM $L_{670\,nm}$ and AERONET $L_{675\,nm}$ measurements. CC denotes the correlation coefficient, LS the least-squares affine regression and PCA the first component in principal component analysis.

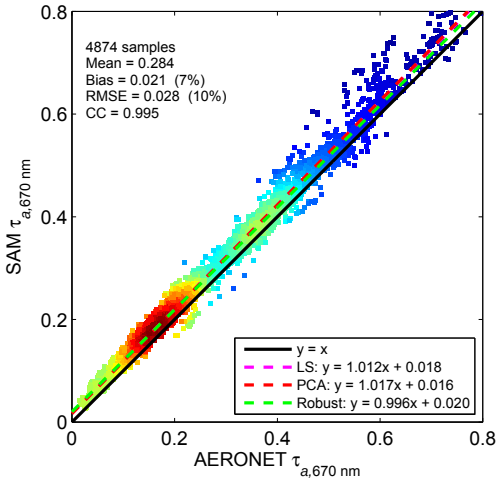

Figure 2. Scatter density plot between the SAM and AERONET $\tau_{a,670\,nm}$. The axes are limited to 0.8 for a better view.

sults are good, implying reliable measurements from both instruments. The AERONET measurements were collected at 675 nm while those of SAM were collected at 670 nm. This may induce minor errors in this comparison. Also shown in Fig. 1 are the mean value of the observables on the x axis, the correlation coefficient, the 1 : 1 line, the least-squares affine regression, the robust affine regression and the first axis of inertia, also known as the first component in principal component analysis.

The AERONET AOD is not provided at the specific wavelength of the SAM instrument of 670 nm. Therefore, the AERONET AOD at this specific wavelength was computed using a second-order polynomial fit of AOD vs. wavelength using the AERONET measurements of AOD in the interval [440, 675 nm] (Eck et al., 1999) as

$$\ln(\tau_{a,\lambda}) = a_0 + a_1 \ln(\lambda) + a_2 \ln(\lambda)^2. \quad (5)$$

This method to compute the reference AOD at 670 nm was selected because the fine-mode pollution aerosols, mainly produced by the petroleum industry in the UAE, affect the linear fit of $\ln(\tau_{a,\lambda})$ vs. $\ln(\lambda)$ (Eck et al., 2008).

Thus, 5024 pairs of coincident observations remain, for which the maximum difference in the time stamp of both instruments is 1 min. Similar to the cross-comparison of the radiance measurements to remove potentially cloud-contaminated measurements, the standard deviation of the differences between these remaining pairs of observations was computed. All coinciding samples with a difference greater than three times the standard deviation were filtered out. Out of 5024 pairs of samples, 150 pairs were excluded.

Figure 2 exhibits the density scatter plot of the 4874 pairs of SAM vs. AERONET AOD at 670 nm. The relative RMSE is 10 % and the relative bias is +7 % meaning that the SAM $\tau_{a,670\,nm}$ is greater in average than the AERONET $\tau_{a,670\,nm}$. The R^2 value is high at 0.990. Even though AOD values sometimes exceed 0.8, the limits of the axes have been set to have a maximum value of 0.8 in order to better examine the regions with higher sample densities.

There are several interpretations for the discrepancies observed between the SAM and AERONET $\tau_{a,670\,nm}$. The difference in the field of view of both instruments may partially explain such discrepancies, where the AERONET Sun photometer has an aperture half-angle of 0.6°. This implies a portion of the circumsolar radiation is intercepted within the field of view of the instrument, hence a smaller AOD than that observed by SAM. Although in Sinyuk et al. (2012) the error due to the field of view is quantified to be significantly less (< 0.003 for $\tau_{a,440\,nm} < 0.8$) than the uncertainty in the AERONET AOD retrievals, with 0.01 for $\lambda > 440$ nm.

Another possible cause for such discrepancies is how the Rayleigh scattering and small atmospheric absorption is accounted for at 670 nm in the SAM AOD retrievals. A fixed correction of −0.0556 is used, which was derived empirically by cross calibrations between SAM and AERONET using measurements collected in Oklahoma, USA (J. DeVore and A. LePage, personal communication, 2015). This fixed correction may induce errors in the SAM AOD retrievals, but it is stated by the team at Visidyne Inc. to be less than the uncertainty of the SAM AOD, being 0.03. Indeed, the bias of 0.02 between AERONET and SAM AOD retrievals is less than the reported uncertainty of the SAM AOD.

After running the series of tests on the SAM data, matching the SAM and AERONET data and removing the outliers of the AOD from both instruments (i.e. the 150 samples of the originally matched 5024 samples), two main data sets remain which are used in the remainder of this article.

i. Data set 1, abbreviated as DS1, already used in Fig. 2 for the AOD comparison. It comprises 4874 observa-

tions of the SAM beam and circumsolar radiance measurements along with their corresponding AERONET $\tau_{a,\lambda}$ and total column content in water vapour, extracted from the DSA Level 2.0 product. There is no data for August 2012 and May 2013. The number of samples varies from a minimum of 102 in July 2012 to a maximum of 809 achieved in September 2012. DS1 is used in the following when modelling the monochromatic $\mathrm{DNI_S}$ with the RTMs.

ii. Data set 2, abbreviated as DS2, comprises 498 observations of the SAM beam and circumsolar radiance measurements along with their corresponding AERONET $\tau_{a,\lambda}$, total column content in water vapour, $P_{a,\lambda}(\xi)$ and g_λ, extracted from the Version 2 inversion products in Level 2.0. A mean value of 0.954 for $\omega_{a,675\,\mathrm{nm}}$ is used along with DS2. There is no data for August 2012 and May 2013 in DS2. Whereas for the remaining 10 months the number of samples varies from a minimum of 14 in July 2012 to a maximum of 103 in March 2013. DS2 is used when modelling the monochromatic CSNI with the RTMs.

The Fig. 3 displays the days of the study period which comprise coinciding SAM and AERONET observations. It illustrates the periods with data available in DS1 and DS2.

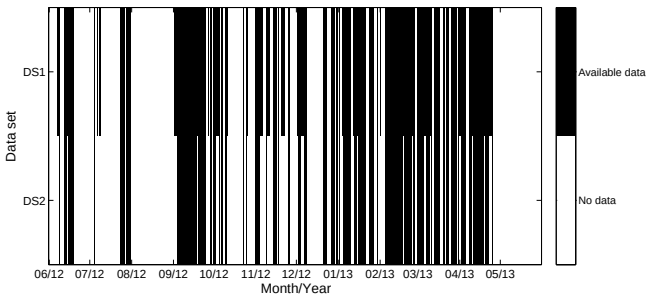

Figure 3. The days of data sets DS1 and DS2 which comprise coinciding AERONET and SAM data.

6 AERONET data in the parameterizations of the radiative transfer models

The AERONET parts of the two data sets are used as input to a RTM which in turn delivers the monochromatic $\mathrm{DNI_S}$ and CSNI which are compared against SAM measurements. Two different RTMs were used: libRadtran and SMARTS.

The Monte Carlo radiative transfer solver MYSTIC available in libRadtran which was used by Reinhardt (2013) and Reinhardt et al. (2014) assumes 3-D geometry and that the Sun is an extended source with a finite diameter. However, these options are not available in the publicly available MYSTIC solver, which can only compute the radiance at one viewing direction at a time. Therefore, in this work the DISORT (DIScrete ORdinates Radiative Transfer; Stamnes et al., 1998, 2000) solver was used in libRadtran version 1.7. It solves the radiative transfer equation in 1-D geometry assuming a plane-parallel atmosphere and allows accurate calculations of the radiance and irradiance. One main advantage of DISORT is that it allows for the computation of the radiance at multiple viewing directions using one input file.

SMARTS is a physical model able to predict either the monochromatic or broadband direct, diffuse and global irradiances received on the surface of the Earth (Gueymard, 1995, 2001). It is also capable of simulating the irradiance that would be measured by a radiometer by defining the viewing angles of the radiometer.

Both SMARTS and libRadtran assume the solar disc is a point source, i.e. a Dirac function. Therefore, the monochromatic $\mathrm{DNI_S}$ is provided as a direct output by both RTMs.

In libRadtran the diffuse radiance is modelled at the viewing angles specified by the user. Therefore, in the cases of the libRadtran outputs and SAM measurements the monochromatic CSNI is computed by Eq. (4) in the interval [$\delta = 0.52°$, $\alpha = 6°$]. In SMARTS the monochromatic CSNI is an output of the model. Therefore, to compute the CSNI from SMARTS in this same interval the code is run twice, once to compute the CSNI up to 6° and once up to 0.52° and then the finally investigated CSNI is their difference.

The parameterizations of the two RTMs are presented in the following sections.

6.1 libRadtran

libRadtran offers the flexibility of a user-defined $P_{a,\lambda}(\xi)$. $P_{a,\lambda}(\xi)$ can be expressed as a series of Legendre polynomials:

$$p_0(x) = 1,\, p_l(x) = \frac{1}{(2^l l!)}\frac{\mathrm{d}^l}{\mathrm{d}x^l}(x^2-1)^l \mathrm{for} l = 1, 2, \ldots, \quad (6)$$

where p_l is the l'th Legendre polynomial as a function of x (Courant and Hilbert, 1953). One way is to use the *pmom* tool in libRadtran that computes the Legendre moments of the measured $P_{a,\lambda}(\xi)$ (Mayer et al., 2012). It takes hundreds of Legendre moments to describe $P_{a,\lambda}(\xi)$ with a sufficient accuracy, especially for small values of ξ.

Practically, the simplest and most common representation of $P_{a,\lambda}(\xi)$ is the Henyey–Greenstein (HG) phase function, which is based on g_λ only (Henyey and Greenstein, 1941; Liou, 2002):

$$P_{\mathrm{HG}}(\xi, g) = (1-g^2)/(1+g^2-2g\cos(\xi))^{1.5}, \quad (7)$$

where P_{HG} is the HG phase function and g is the asymmetry parameter, to be replaced with g_λ for monochromatic phase functions.

However, the HG phase function does not properly reproduce the scattering patterns which are strongly peaked in the forward direction (Liou, 2002). An accurate representation of

the sharp peaks of $P_{a,\lambda}(\xi)$ is very important for an accurate estimate of the circumsolar diffuse monochromatic radiance.

Irvine (1965) and Kattawar (1975) proposed a two-term HG (TTHG) phase function to better depict phase functions with sharp peaks. To the best of the knowledge of the authors, no articles have been found on the direct application of the TTHG phase function to model the circumsolar radiation under turbid cloud-free skies. The TTHG phase function is computed as (Haltrin, 2002; Kattawar, 1975)

$$P_{\mathrm{TTHG}}(\xi, c_1, c_2, c_3) = c_1 P_{\mathrm{HG}}(\xi, c_2) + (1 - c_1) P_{\mathrm{HG}}(\xi, c_3), \quad (8)$$

where P_{TTHG} is the TTHG phase function and c_1, c_2 and c_3 are three parameters describing P_{TTHG}. In this study each AERONET $P_{a,\lambda}(\xi)$ was used to fit the three parameters c_1, c_2 and c_3 of Eq. (6) using the nonlinear least-squares Levenberg–Marquardt method (Marquardt, 1963).

Practically, the RTM libRadtran expects Legendre moments. Therefore, knowing the c_1, c_2 and c_3 parameters, the TTHG phase function must be expanded as a series of Legendre polynomials as

$$P_{\mathrm{TTHG}}(\xi, c_1, c_2, c_3) = \sum_{l=0}^{\infty} (2l+1)(c_1 c_2^l + (1 - c_1) c_3^l) p_l(\cos(\xi)), \quad (9)$$

where $(c_1 c_2^l + (1 - c_1) c_3^l)$ is the l'th Legendre moment and p_l is the l'th Legendre polynomial as a function of $\cos(\xi)$, to compute hundreds of Legendre moments before passing them on to libRadtran.

The following were the specific inputs to libRadtran:

i. θ_{S}, computed by the SG2 algorithm of Blanc and Wald (2012);

ii. $\lambda = 670\,\mathrm{nm}$, to compute the corresponding monochromatic radiance/irradiance;

iii. $\tau_{a,670\,\mathrm{nm}}$, computed as per Eq. (5);

iv. the total column content in water vapour;

v. $\omega_{a,675\,\mathrm{nm}}$, only needed for radiance modelling;

vi. the moments of the $P_{a,675\,\mathrm{nm}}(\xi)$, only needed for radiance modelling;

vii. the mid-latitude summer atmospheric profile from Anderson et al. (1986);

viii. the extraterrestrial spectrum of Gueymard (2004), which is the same one available in SMARTS;

ix. the day of the year, i.e. 1 to 365 or 366 for a leap year, to correct for the Sun–Earth distance;

x. the altitude of the site above mean sea level;

xi. the altitude of the sensor above ground level;

xii. the sky element zenith angle θ;

xiii. the sky element azimuth angle φ;

xiv. the radiative transfer equation solver, DISORT;

xv. default value of 16 for the number of streams to be used in DISORT. An increase in the number of streams (32 were tested) causes significantly longer computational timings with no effects on the results.

In libRadtran, if the asymmetry parameter $g_{675\,\mathrm{nm}}$ is defined instead of the moments of $P_{a,675\,\mathrm{nm}}(\xi)$, then a HG phase function is assumed. When $\omega_{a,675\,\mathrm{nm}}$ and $P_{a,675\,\mathrm{nm}}(\xi)$ are both not available as inputs, another option is to define the aerosol type and retrieve their corresponding typical values from the OPAC (Optical Properties of Aerosols and Clouds) library (Hess et al., 1998; Mayer and Kylling, 2005).

6.2 SMARTS

In the RTM SMARTS (Gueymard, 2005) the specific inputs were

i. the pressure at the site, defined by the latitude, the altitude of the site above mean sea level and the altitude of the sensor above ground level;

ii. the atmospheric profile, chosen as mid-latitude summer;

iii. the total column content in water vapour;

iv. the extraterrestrial spectrum, selected as Gueymard (2004);

v. the aerosol model. Once it was selected as "DESERT_MAX" and once it was user-defined by providing

1. Ångström wavelength exponent for wavelength less than 500 nm,

2. Ångström wavelength exponent for wavelength greater than 500 nm,

3. the aerosol single scattering albedo and

4. the asymmetry parameter;

vi. turbidity data. Selected as $\tau_{a,500\,\mathrm{nm}}$, extracted directly from the AERONET products;

vii. aperture half-angle α of the instrument;

viii. the solar position.

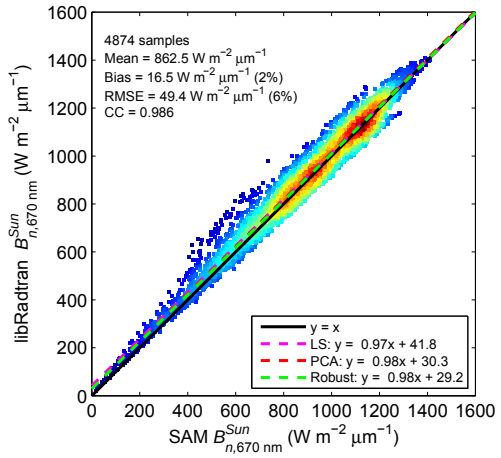

Figure 4. Scatter density plot of the libRadtran DNI_S at 670 nm (libRadtran $B^{Sun}_{n,670\,nm}$) vs. the reference values from the SAM instrument (SAM $B^{Sun}_{n,670\,nm}$).

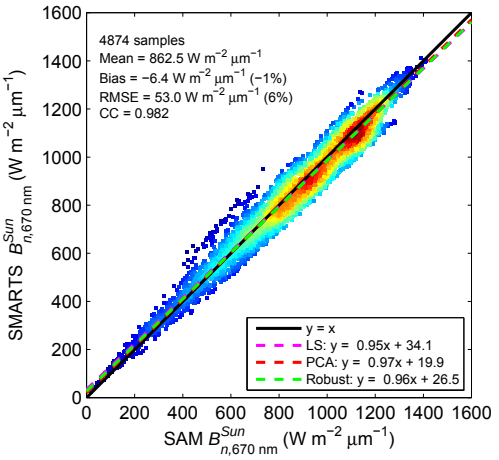

Figure 5. Scatter density plot of the SMARTS DNI_S at 670 nm (SMARTS $B^{Sun}_{n,670\,nm}$) vs. the reference values from the SAM instrument (SAM $B^{Sun}_{n,670\,nm}$).

When using the user-defined aerosol model in SMARTS, it requires the broadband asymmetry parameter and the broadband aerosol single scattering albedo, but such broadband values were not available. Therefore, to model the monochromatic CSNI $g_{675\,nm}$ was used from data set DS2, and to model the monochromatic DNI_S the mean value of $g_{675\,nm}$ from the AERONET data was used. In both cases the mean value of $\omega_{a,675\,nm}$ was used. Also, it is not possible to specify $P_{a,\lambda}(\xi)$ in the SMARTS version 2.9.5, which is automatically selected from tables when selecting the aerosol model.

7 Results and discussion

The results of the modelled DNI_S at 670 nm of data set DS1 are presented in Table 2. Both RTMs exhibit a relative RMSE of 6 %. The relative bias obtained by libRadtran is +2 %, whereas that of SMARTS is −1 %. The R^2 is 0.972 for libRadtran and 0.964 for SMARTS. The scatter density plots are exhibited in Figs. 4 (libRadtran) and 5 (SMARTS). The same atmospheric profile (mid-latitude summer) was defined in both RTMs. The difference in the bias between both models may be due to the scaling of $\tau_{a,670\,nm}$. In libRadtran $\tau_{a,670\,nm}$ was computed using Eq. (5), whereas in SMARTS $\tau_{a,670\,nm}$ is scaled from $\tau_{a,500\,nm}$ using the Ångström exponents provided as input. Other sources of errors in both the SMARTS and libRadtran estimates may be due to a miscalibration of the AERONET Sun photometer or misalignments in its tracking mechanism (Dubovik et al., 2000).

Although there is no observable pattern in the monthly bias, the bias is largest during the summer month of July 2013 (+9 % from libRadtran and +5 % from SMARTS). This bias is attributed to the turbid atmosphere present during this month, which possibly means more soiling on the entrance window of the SAM instrument and hence an underestimation in the SAM measurements or in other words an overestimation in the modelled values. Indeed, by observing the monthly means of the AERONET $\tau_{a,675\,nm}$ of data set DS1 the largest value is obtained during July 2013, with a value of 0.600.

There is also a suspicious behaviour in the bias from the month of November to December 2012, where the relative bias changes signs from −4 % to +6 % respectively for the libRadtran modelled values and from −8 % to +2 % respectively for the SMARTS modelled values. This sudden change in bias is mainly attributed to a broken entrance window for the SAM instrument for some time during November 2012 (Wilbert, 2014).

For the overall data set, it may be concluded that both models provide very accurate estimates of the monochromatic DNI_S, where the uncertainty of the SAM instrument in the solar disc region is 1 % for $\tau_{a,670\,nm} < 0.6$.

The modelling of the CSNI at 670 nm of data set DS2 in the interval $[\delta = 0.52°, \alpha = 6°]$ is very strongly dependent on the defined aerosol optical properties. The differences in the results by applying different inputs to the RTMs are summarized in Table 3.

There are several problems concerning a fair comparison of the results of libRadtran and SMARTS. One is that SMARTS does not give the flexibility to input $\tau_{a,\lambda}$ at a user-defined wavelength except at 500, 550 or 1000 nm (although compensated for by the Ångström exponents), whereas this flexibility is available in libRadtran. Also, SMARTS, at least the publicly available version, does not offer the flexibility of a user-defined $P_{a,\lambda}(\xi)$, while that option is available in libRadtran with the Legendre moments.

It is clear from the results that the HG phase function is a very bad representation of $P_{a,\lambda}(\xi)$ and its use is not recommended when modelling the CSNI, in a desert environment

Table 2. Results of libRadtran and SMARTS of data set DS1 for the modelling of the monochromatic DNI_S at 670 nm.

RTM	Aerosol optical properties	Mean	Bias		RMSE		R^2
		$W\,m^{-2}\,\mu m^{-1}$	$W\,m^{-2}\,\mu m^{-1}$	%	$W\,m^{-2}\,\mu m^{-1}$	%	
libRadtran	$\tau_{a,670\,nm}$	862.5	+16.5	+2	49.4	6	0.972
SMARTS	$\tau_{a,500\,nm}$	862.5	−6.4	−1	52.0	6	0.964

Table 3. Results of libRadtran and SMARTS of data set DS2 for the modelling of the monochromatic CSNI in the interval [$\delta = 0.52°$, $\alpha = 6°$] at 670 nm.

RTM	Aerosol optical properties	Mean	Bias		RMSE		R^2
		$W\,m^{-2}\,\mu m^{-1}$	$W\,m^{-2}\,\mu m^{-1}$	%	$W\,m^{-2}\,\mu m^{-1}$	%	
libRadtran	$\tau_{a,670\,nm}$; mean $\omega_{a,675\,nm}$; HG phase function: $g_{675\,nm}$	88.1	−68.1	−77	72.6	82	0.726
SMARTS	$\tau_{a,500\,nm}$; mean $\omega_{a,675\,nm}$; $g_{675\,nm}$	88.1	−64.6	−73	69.7	79	0.667
libRadtran	$\tau_{a,670\,nm}$; OPAC desert type aerosol	88.1	−33.5	−38	38.7	44	0.711
SMARTS	$\tau_{a,500\,nm}$; "DESERT_MAX" aerosol model	88.1	−41.9	−48	48.8	55	0.514
libRadtran	$\tau_{a,670\,nm}$; mean $\omega_{a,675\,nm}$; TTHG phase function	88.1	−21.4	−24	24.2	27	0.882

at least. Even though R^2 is not too low, 0.726 for libRadtran and 0.667 for SMARTS, a very large negative relative bias is observed in both RTMs when the HG phase function is used.

In the case when using the aerosol models of the predefined libraries available in the RTMs, the bias significantly improves when compared to using the HG phase function but still remains negative. However, R^2 becomes lower. When selecting the desert type aerosol of the OPAC library in libRadtran the relative RMSE is 44 %, the relative bias is −38 % and R^2 is 0.711. Selecting the 'DESERT_MAX' aerosol type in SMARTS the relative RMSE is 55 %, the relative bias is −41 % and R^2 is 0.514. The errors are still high though, and neither the "DESERT_MAX" aerosol model in SMARTS nor the desert type aerosol of the OPAC library in libRadtran provides accurate results of the monochromatic CSNI under cloud-free conditions over the study area.

The underestimation of the circumsolar effect by SMARTS may partly be explained by an incorrect phase function that was hard-coded for all desert aerosol types in v2.9.5 of the code (C. A. Gueymard, personal communication, 2015). The large underestimation of the DESERT_MAX single scattering albedo, 0.7 as opposed to the mean value from AERONET of 0.954, also contributes to the observed bias.

As for libRadtran, the aerosol optical properties extracted from the OPAC library are in fact not too far off from the AERONET means: $g_{675\,nm} \approx 0.71$ and $\omega_{a,675\,nm} \approx 0.91$ as opposed to the mean values from AERONET of 0.699 and 0.954 respectively. The OPAC properties are not provided at the exact wavelength of interest but were determined by observing the values provided at 650 and 700 nm at a relative humidity of 70 and 80 % (http://andromeda.caf.dlr.de/data-products/spectroscopy-data/optical-properties-aerosols-and-clouds-opac). These values of relative humidity were selected based on the relative humidity at the surface for the mid-latitude summer profile, which is 75.7 % (cf. Table 3.1 in Gueymard, 1995). This implies that the aerosol phase function computed by libRadtran using the OPAC desert model is not able to depict the sharp peaks at the smallest ξ.

When using the TTHG phase function determined from the AERONET measurements instead of the HG function, all statistical indicators show a very significant improvement. The scatter density plot for this case is exhibited in Fig. 6. The relative RMSE is 27 %, the relative bias is −24 % and R^2 is 0.882. The underestimation is nevertheless still non-negligible. This bias may partly originate from the phase function $P_{a,675\,nm}(\xi)$ used as input. The aperture half-angle of the Sun photometer used in the AERONET stations is 0.6°, which is relatively large considering that the angular radius of the solar disc is 0.266° ± 1.7 %, and that the circumsolar region in this context is defined up to 6°. In fact, for $\xi < 6°$ the AERONET $P_{a,675\,nm}(\xi)$ is only provided at three ξ: 0, 1.71 and 3.93°. In addition, $P_{a,675\,nm}(\xi)$ at the first two ξ are assumed to be extrapolated values, because in the AERONET Version 2 inversion products only almucantar radiance measurements for $\xi \geq 3.2°$ are considered (Holben et al., 2006). This is a limitation of using the AERONET $P_{a,675\,nm}(\xi)$.

Other errors may in fact be due to the reference SAM measurements. For example, the monthly relative bias for November 2012 from the radiance measurements comparison (cf. Fig. 1) is +23 %, where the SAM radiance mea-

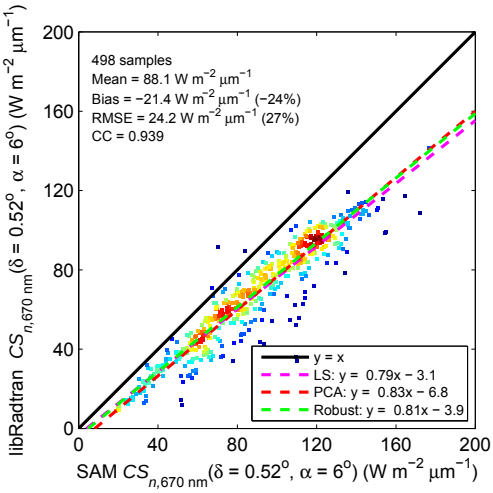

Figure 6. Scatter density plot of the libRadtran CSNI at 670 nm modelled by defining the TTHG phase function (libRadtran $CS_{n,670\,nm}(\delta = 0.52°, \alpha = 6°)$) vs. the reference values from the SAM instrument (SAM $CS_{n,670\,nm}(\delta = 0.52°, \alpha = 6°)$).

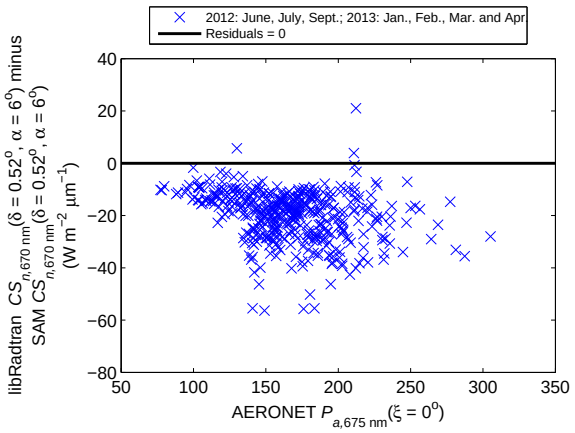

Figure 7. Residuals (libRadtran CSNI at 670 nm modelled by defining the TTHG phase function minus the SAM reference CSNI at 670 nm) vs. the AERONET aerosol phase function at ξ of 0° (AERONET $P_{a,675\,nm}(\xi = 0°)$) for June, July and September 2012 and January, February, March and April 2013.

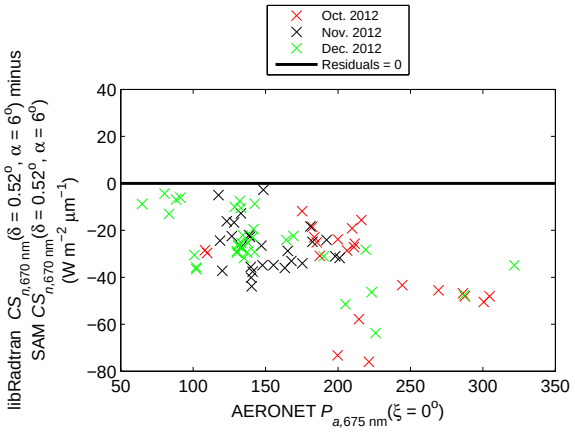

Figure 8. Residuals (libRadtran CSNI at 670 nm modelled by defining the TTHG phase function minus the SAM reference CSNI at 670 nm) vs. the AERONET aerosol phase function at ξ of 0° (AERONET $P_{a,675\,nm}(\xi = 0°)$) for October, November and December 2012.

surements are overestimated in average with respect to the AERONET radiance measurements. This comparison for November agrees with the similar comparison performed by Wilbert (2014) and is partly explained by the broken entrance window of the SAM instrument. This would in turn induce a larger underestimation in the CSNI in this month.

Indeed, it is observed that the CSNI is underestimated in November 2012 by −39 %. Other months exhibiting large underestimations in the estimated CSNI are October and December 2012, with a relative bias of −38 and −37 % respectively. The remaining months have a bias ranging from −24 to −20 % (excluding August 2012 and May 2013 which have no observations).

The residuals of the libRadtran and SAM monochromatic CSNI vs. the AERONET $P_{a,675\,nm}(\xi = 0°)$ are exhibited in Fig. 7 for the months of June, July and September 2012 and January, February, March and April 2013 and Fig. 8 for the months of October, November, December 2012. Although the number of samples is relatively low for the AERONET $P_{a,675\,nm}(\xi = 0°)$ with the sharpest peaks, it is evident that the underestimation is greater in the negative direction for the AERONET $P_{a,675\,nm}(\xi = 0°)$ with the sharpest peaks. This observation supports the hypothesis that the AERONET $P_{a,675\,nm}(\xi)$ might not be very accurate for the smallest ξ, especially for those with the sharpest peaks. It is also evident in Fig. 8 that the larger underestimation of October and December 2012 is due to the underestimation in the libRadtran monochromatic CSNI for the $P_{a,675\,nm}$ with the sharper peaks. However, the same cannot be said for November 2012, because $P_{a,675\,nm}(\xi = 0°)$ has relatively moderate values but the modelled libRadtran monochromatic CSNI generally exhibit a larger underestimation than other samples with similar values of $P_{a,675\,nm}(\xi = 0°)$. Again this is due to an overestimation in the SAM radiance measurements for this month.

Another source of error may be that in the AERONET Version 2 inversion products, including $P_{a,675\,nm}(\xi)$ and $\omega_{a,675\,nm}$, the aerosol particle shapes are assumed to be composed of spheres (Dubovik and King, 2000) and spheroids (Dubovik et al., 2002). However, in reality, dust particles have a variety of shapes, not necessarily spheroids, and this may affect the accuracy of the retrieved AERONET aerosol optical properties (Dubovik et al., 2006; Kahnert and Nousiainen, 2006). Nevertheless, given the uncertainty of the SAM instrument in the aureole region to be ∼ 15 %, it is concluded that defining the moments of the TTHG phase function in libRadtran provides an overall remarkably accurate and in-

teresting estimates of the monochromatic CSNI under cloud-free conditions over the study area.

8 Conclusions

AERONET data may very well be used to accurately model the monochromatic beam and circumsolar irradiances under cloud-free conditions in desert environment. In modelling the DNI_S at 670 nm both libRadtran and SMARTS provide very similar results. The relative RMSE is 6 % for both RTMs, while the relative bias is +2 % for libRadtran and −1 % for SMARTS, and R^2 is 0.972 and 0.964 in the same order. For modelling the CSNI at 670 nm in the interval [$\delta = 0.52°$, $\alpha = 6°$] five different configurations of inputs have been tested, two using SMARTS and three using libRadtran. Of the tested configurations, the most accurate is that using libRadtran when the aerosol phase function $P_{a,675\,\mathrm{nm}}(\xi)$ is defined as a three-parameter TTHG phase function. In this case, the relative RMSE is 27 %, relative bias is −24 % and R^2 is 0.882.

The underestimation of the modelled CSNI is mainly attributed to errors in the SAM reference measurements and the AERONET aerosol phase function. It is believed that a better representation of the aerosol phase function $P_{a,675\,\mathrm{nm}}(\xi)$ for the smallest ξ than the one provided by AERONET would further improve the modelling results of the CSNI. Given the uncertainty of the SAM radiance measurements in the aureole region to be ∼ 15 %, it is safe to say that the methodology presented herein provides a very accurate estimate of the CSNI.

The results of the modelling of the CSNI are significantly better than those obtained when representing $P_{a,675\,\mathrm{nm}}(\xi)$ as a HG phase function or when using the libraries of aerosol optical properties available in both libRadtran and SMARTS. It is therefore not recommended to use such parameterizations when modelling the CSNI in a desert environment.

Normally, one should be able to model the monochromatic beam and circumsolar irradiances using the corresponding AERONET data and the presented methodology over any environment. The validations in this study were only performed in a desert environment. The choice of using a mean representative value of the single scattering albedo over other environments is a point which should be addressed first.

In the work leading up to these results several other procedures have been proposed. Firstly, the work exploits measurements made by the SAM instrument. It is fairly new, and no well-established procedure has been published to check the quality of the measurements. Several elements were developed here that may further contribute to a quality-control procedure, whose design requires more work. Secondly, modelling the AERONET phase function $P_{a,\lambda}(\xi)$ as a TTHG phase function to compute the CSNI under cloud-free conditions is proposed. This representation has the advantage of accurately reproducing the sharp peaks of $P_{a,\lambda}(\xi)$ for the smallest ξ, whilst being represented by only three parameters. This opens up the path for a model to be developed to estimate the three parameters of the phase function, rather than estimating the hundreds of Legendre moments required to accurately represent the phase function.

The next step is to apply this approach to model the broadband DNI_S and CSNI. This would directly contribute to the recommendation of Blanc et al. (2014) to report the sunshape and circumsolar ratio with the standard DNI measurements. A further step may then be to integrate the model of Reinhardt (2013) and Reinhardt et al. (2014) to devise a model which works under both cloud-free and cirrus cloudy conditions.

Acknowledgements. The research leading to these results has received funding from Total New Energies in the framework of the PREDISOL project and from the French Agency ADEME in charge of energy (grant no. 1105C0028, 2011–2016), and took place within the Task 46 “solar resource assessment and forecasting” of the Solar Heating and Cooling programme of the International Energy Agency. The authors thank the team developing libRadtran and C.A. Gueymard for developing SMARTS and for the discussions which took place with him. The authors also thank the PI(s) of the Masdar AERONET (P. Armstrong and M. Chiesa) and SAM (P. Armstrong) stations, along with all the personnel who installed and maintained the instruments. The authors are appreciative of all the efforts of S. Wilbert and the four other anonymous reviewers; their invaluable comments and contributions were key in the development of this manuscript. Last but not least, the authors thank J. DeVore, A. LePage, A. T. Stair and D. Villanucci from Visidyne Inc. for the discussion regarding the SAM measurements and retrievals.

Edited by: A. Sayer

References

Anderson, G. P., Clough, S. A., Kneizys, F. X., Chetwynd, J. H., and Shettle, E. P.: AFGL atmospheric constituent profiles (0–120 km), Tech. Rep. AFGL-TR-86-0110, Air Force Geophys. Lab., Hanscom Air Force Base, Bedford, Mass., USA, available at: http://www.dtic.mil/cgi-bin/GetTRDoc?AD=ADA175173 (last access: 3 December 2015), 1986.

Blanc, P. and Wald, L.: The SG2 algorithm for a fast and accurate computation of the position of the Sun for multi-decadal time period, Sol. Energy, 86, 3072–3083, doi:10.1016/j.solener.2012.07.018, 2012.

Blanc, P., Espinar, B., Geuder, N., Gueymard, C. A., Meyer, R., Pitz-Paal, R., Reinhardt, B., Renné, D., Sengupta, M., Wald, L., and Wilbert, S.: Direct normal irradiance related definitions and applications: The circumsolar issue, Sol. Energy, 110, 561–577, doi:10.1016/j.solener.2014.10.001, 2014.

Brand, B. and Zingerle, J.: The renewable energy targets of the Maghreb countries: Impact on electricity supply and conventional power markets, Energy Policy, 39, 4411–4419, doi:10.1016/j.enpol.2010.10.010, 2011.

Buie, D., Monger, A. G., and Dey, C. J.: Sunshape distributions for terrestrial solar simulations, Sol. Energy, 74, 113–122, doi:10.1016/S0038-092X(03)00125-7, 2003.

Courant, R. and Hilbert, D.: Methods of mathematical physics, Interscience Publishers, Inc., New York, 82–83, 1953.

DeVore, J. G., Stair, A. T., and McClatchey, R.: SAM (sun and aureole measurement): Examples from April 06 IOP at SGP, poster for the Atmospheric Radiation Measurement Program, available at: http://www.arm.gov/publications/proceedings/conf17/poster/P00021.pdf (last access: 3 December 2015), 2007.

DeVore, J. G., Stair, Jr., A. T., LePage, A., and Villanucci, D.: Using scattering calculations to compare MODIS retrievals of thin cirrus optical properties with SAM solar disk and aureole radiance measurements, J. Geophys. Res., 117, 1–11, doi:10.1029/2011JD015858, 2012a.

DeVore, J. G., Villanucci, D., and LePage, A.: Aureolegraph internal scattering correction, Appl. Opt., 51, 7891–7899, doi:10.1364/AO.51.007891, 2012b.

Dubovik, O. and King, M. D.: A flexible inversion algorithm for retrieval of aerosol optical properties from Sun and sky radiance measurements, J. Geophys. Res., 105, 20673–20696, doi:10.1029/2000JD900282, 2000.

Dubovik, O., Smirnov, A., Holben, B. N., King, M. D., Kaufman, Y. J., Eck, T. F., and Slutsker, I.: Accuracy assessments of aerosol optical properties retrieved from Aerosol Robotic Network (AERONET) Sun and sky radiance measurements, J. Geophys. Res., 105, 9791–9806, doi:10.1029/2000JD900040, 2000.

Dubovik, O., Holben, B. N., Lapyonok, T., Sinyuk, A., Mishchenko, M., Yang, P., and Slutsker, I.: Non-spherical aerosol retrieval method employing light scattering by spheroids, Geophys. Res. Lett., 29, 1–4, doi:10.1029/2001GL014506, 2002.

Dubovik, O., Sinyuk, A., Lapyonok, T., Holben, B. N., Mishchenko, M., Yang, P., Eck, T. F., Volten, H., Muñoz, O., Veihelmann, B., van der Zande, W. J., Leon, J. F., Sorokin, M., and Slutsker, I.: Application of spheroid models to account for aerosol particle nonsphericity in remote sensing of desert dust, J. Geophys. Res.-Atmos., 111, D11208, doi:10.1029/2005JD006619, 2006.

Eck, T. F., Holben, B. N., Reid, J. S., Dubovik, O., Smirnov, A., Neill, N. T. O., Slutsker, I., and Kinne, S.: Wavelength dependence of the optical depth of biomass burning, urban, and desert dust aerosols, J. Geophys. Res., 104, 31333–31349, doi:10.1029/1999JD900923, 1999.

Eck, T. F., Holben, B. N., Reid, J. S., Sinyuk, A., Dubovik, O., Smirnov, A., Giles, D., O'Neill, N. T., Tsay, S. C., Ji, Q., Al Mandoos, A., Ramzan Khan, M., Reid, E. A., Schafer, J. S., Sorokine, M., Newcomb, W., and Slutsker, I.: Spatial and temporal variability of column-integrated aerosol optical properties in the southern Arabian Gulf and United Arab Emirates in summer, J. Geophys. Res.-Atmos., 113, 1–19, doi:10.1029/2007JD008944, 2008.

Eilers, P. H. C. and Goeman, J. J.: Enhancing scatterplots with smoothed densities, Bioinformatics, 20, 623–628, doi:10.1093/bioinformatics/btg454, 2004.

Eissa, Y., Blanc, P., Oumbe, A., Ghedira, H., and Wald, L.: Estimation of the circumsolar ratio in a turbid atmosphere, Energy Procedia, 57, 1169–1178, doi:10.1016/j.egypro.2014.10.104, 2014.

Gherboudj, I. and Ghedira, H.: Spatiotemporal assessment of dust loading over the United Arab Emirates, Int. J. Climatol., 32, 3321–3335, doi:10.1002/joc.3909, 2014.

Griffiths, S.: Strategic considerations for deployment of solar photovoltaics in the Middle East and North Africa, Energy Strateg. Rev., 2, 125–131, doi:10.1016/j.esr.2012.11.001, 2013.

Gueymard, C. A.: Simple Model of the Atmospheric Radiative Transfer of Sunshine, version 2 (SMARTS2): Algorithms description and performance assessment, Report FSEC-PF-270-95, Florida Solar Energy Center, available at: http://www.fsec.ucf.edu/en/publications/pdf/FSEC-PF-270-95.pdf (last access: 3 December 2015), 1995.

Gueymard, C. A.: Parameterized transmittance model for direct beam and circumsolar spectral irradiance, Sol. Energy, 71, 325–346, doi:10.1016/S0038-092X(01)00054-8, 2001.

Gueymard, C. A.: The sun's total and spectral irradiance for solar energy applications and solar radiation models, Sol. Energy, 76, 423–453, doi:10.1016/j.solener.2003.08.039, 2004.

Gueymard, C. A.: SMARTS code, version 2.9.5: User's manual, available at: http://rredc.nrel.gov/solar/models/smarts/relatedrefs/smarts295_users_manual_pc.pdf (last access: 3 December 2015), 2005.

Haltrin, V. I.: One-parameter two-term Henyey-Greenstein phase function for light scattering in seawater, Appl. Opt., 41, 1022–1028, doi:10.1364/AO.41.001022, 2002.

Henyey, L. G. and Greenstein, J. L.: Diffuse radiation in the galaxy, Astrophys. J., 93, 70–83, 1941.

Hess, M., Koepke, P., and Schult, I.: Optical Properties of Aerosols and Clouds: The software package OPAC, B. Am. Meteorol. Soc., 79, 831–844, doi:10.1175/1520-0477(1998)079<0831:OPOAAC>2.0.CO;2, 1998.

Holben, B. N., Eck, T. F., Slutsker, I., Tanre, D., Buis, J. P., Setzer, A., Vermote, E., Reagan, J. A., Kaufman, Y. J., Nakajima, T., Lavenu, F., Jankowiak, I., and Smirnov, A.: AERONET – A federated instrument network and data archive for aerosol characterization, Remote Sens. Environ., 66, 1–16, doi:10.1016/S0034-4257(98)00031-5, 1998.

Holben, B. N., Tanré, D., Smirnov, A., Eck, T. F., Slutsker, I., Abuhassan, N., Newcomb, W. W., Schafer, J. S., Chatenet, B., Lavenu, F., Kaufman, Y. J., Castle, J. Vande, Setzer, A., Markham, B., Clark, D., Frouin, R., Halthore, R., Karneli, A., O'Neill, N. T., Pietras, C., Pinker, R. T., Voss, K., and Zibordi, G.: An emerging ground-based aerosol climatology: Aerosol optical depth from AERONET, J. Geophys. Res.-Atmos., 106, 12067–12097, doi:10.1029/2001JD900014, 2001.

Holben, B. N., Eck, T. F., Slutsker, I., Smirnov, A., Sinyuk, A., Schafer, J., Giles, D., and Dubovik, O.: AERONET's Version 2.0 quality assurance criteria, Proc. SPIE 6408, Remote Sensing of the Atmosphere and Clouds, 64080Q, doi:10.1117/12.706524, 2006.

Irvine, W. M.: Multiple scattering by large particles, Astrophys. J., 142, 1563–1575, 1965.

ISO-9488: Solar energy – Vocabulary, available at: https://www.iso.org/obp/ui/#iso:std:iso:9488:ed-1:v1:en (last access: 3 December 2015), 1999.

Jilinski, E. G., Puliaev, S. P., Penna, J. L., Andrei, A. H., Sinceac, V., Chollet, F., and Delmas, C.: Solar diameter observations with the Astrolabe at Observatório Nacional – Rio de Janeiro, Astron. Astrophys., 130, 317–321, doi:10.1051/aas:1998228, 1998.

Kahnert, M. and Nousiainen, T.: Uncertainties in measured and modelled asymmetry parameters of mineral dust

aerosols, J. Quant. Spectrosc. Radiat. Transf., 100, 173–178, doi:10.1016/j.jqsrt.2005.11.035, 2006.

Kasten, F. and Young, A. T.: Revised optical air mass tables and approximation formula, Appl. Opt., 28, 4735–4738, doi:10.1364/AO.28.004735, 1989.

Kattawar, G. W.: A three-parameter analytic phase function for multiple scattering calculations, J. Quant. Spectrosc. Radiat. Transf., 15, 839–849, doi:10.1016/0022-4073(75)90095-3, 1975.

LePage, A., Kras, S., and DeVore, J. G.: Description of SAM (sun and aureole measurement) sensor data collected in support of CLASIC and CHAPS, available at: http://www.visidyne.com/SAM/VI-5311(SamClasic+ChapsData).j-2.pdf, 2008.

Liou, K. N.: An Introduction to Atmospheric Radiation, 2nd Edition, Academic Press, 583 pp., 2002.

Marquardt, D. W.: An algorithm for least-squares estimation of nonlinear parameters, J. Soc. Ind. Appl. Math., 11, 431–441, doi:10.1137/0111030, 1963.

Mayer, B. and Kylling, A.: Technical note: The libRadtran software package for radiative transfer calculations – description and examples of use, Atmos. Chem. Phys., 5, 1855–1877, doi:10.5194/acp-5-1855-2005, 2005.

Mayer, B., Kylling, A., Emde, C., Hamann, U., and Buras, R.: libRadtran user's guide, available at: http://www.libradtran.org/download/history/libRadtran-1.7.tar.gz (last access: 3 December 2015), 2012.

Neumann, A., Witzke, A., Jones, S. A., and Schmitt, G.: Representative terrestrial solar brightness profiles, J. Sol. Energy Eng., 124, 198–204, doi:10.1115/1.1464880, 2002.

Noring, J. E., Grether, D. F., and Hunt, A. J.: Circumsolar radiation data: the Lawrence Berkeley Laboratory Reduced Data Base, Berkeley, California, doi:10.2172/10109904, 1991.

Oumbe, A., Qu, Z., Blanc, P., Bru, H., Lefevre, M., and Wald, L.: Modeling circumsolar irradiance to adjust beam irradiances from radiative transfer models to measurements, in EMS Annual Meeting, Lodz, Poland, available at: http://www.endorse-fp7.eu/sites/www.endorse-fp7.eu/files/docs/Poster_EMS2012_CRS_V2.2.pdf (last access: 3 December 2015), 2012.

Reinhardt, B.: On the retrieval of circumsolar radiation from satellite observations and weather model output, PhD thesis, Ludwig-Maximilians-Universität München, Munich, Germany, available at: https://edoc.ub.uni-muenchen.de/16438/1/Reinhardt_Bernhard.pdf (last access: 3 December 2015), 2013.

Reinhardt, B., Buras, R., Bugliaro, L., Wilbert, S., and Mayer, B.: Determination of circumsolar radiation from Meteosat Second Generation, Atmos. Meas. Tech., 7, 823–838, doi:10.5194/amt-7-823-2014, 2014.

Sinyuk, A., Holben, B. N., Smirnov, A., Eck, T. F., Slutsker, I., Schafer, J. S., Giles, D. M., and Sorokin, M.: Assessment of error in aerosol optical depth measured by AERONET due to aerosol forward scattering, Geophys. Res. Lett., 39, 1–5, doi:10.1029/2012GL053894, 2012.

Smirnov, A., Holben, B. N., Eck, T. F., Dubovik, O., and Slutsker, I.: Cloud-screening and quality control algorithms for the AERONET database, Remote Sens. Environ., 73, 337–349, doi:10.1016/S0034-4257(00)00109-7, 2000.

Stair, A. T. and DeVore, J. G.: Sun and Aureole Measurements: A sensor for cloud optical properties and circumsolar radiation, available at: http://www.visidyne.com/SAM/7_VI-5493(SAMTrifold).ppt (last access: 3 December 2015), 2012.

Stamnes, K., Tsay, S. C., Wiscombe, W., and Jayaweera, K.: Numerically stable algorithm for discrete-ordinate-method radiative transfer in multiple scattering and emitting layered media., Appl. Opt., 27, 2502–2509, doi:10.1364/AO.27.002502, 1988.

Stamnes, K., Tsay, S. C., Wiscombe, W., and Laszlo, I.: DISORT, a general-purpose Fortran program for Discrete-Ordinate-Method Radiative Transfer in scattering and emitting layered media: Documentation of methodology, available at: ftp://climate1.gsfc.nasa.gov/ridgway/Multiple_Scatt/DISORTReport1.1.pdf (last access: 3 December 2015), 2000.

Torres, B., Toledano, C., Berjón, A., Fuertes, D., Molina, V., Gonzalez, R., Canini, M., Cachorro, V. E., Goloub, P., Podvin, T., Blarel, L., Dubovik, O., Bennouna, Y., and de Frutos, A. M.: Measurements on pointing error and field of view of Cimel-318 Sun photometers in the scope of AERONET, Atmos. Meas. Tech., 6, 2207–2220, doi:10.5194/amt-6-2207-2013, 2013.

Thomalla, E., Köpke, P., Müller, H., and Quenzel, H.: Circumsolar radiation calculated for various atmospheric conditions, Sol. Energy, 30, 575–587, doi:10.1016/0038-092X(83)90069-5, 1983.

Wilbert, S.: Determination of circumsolar radiation and its effect on concentrating solar power, Ph.D. thesis, Rheinisch-Westfälische Technische Hochschule Aachen University, Aachen, Germany, available at: http://publications.rwth-aachen.de/record/444996/files/5171.pdf (last access: 3 December 2015), 2014.

Wilbert, S., Reinhardt, B., DeVore, J. G., Röger, M., Pitz-Paal, R., Gueymard, C. A., and Buras, R.: Measurement of Solar Radiance Profiles With the Sun and Aureole Measurement System, J. Sol. Energy Eng., 135, 11 pp., doi:10.1115/1.4024244, 2013.

WMO: Guide to meteorological instruments and methods of observation, World Meteorological Organization, WMO-No 8 (2010 update), 7th edn., Geneva, Switzerland, available at: http://library.wmo.int/pmb_ged/wmo_8_en-2012.pdf (last access: 3 December 2015), 2010.

Yin, B., Min, Q., and Joseph, E.: Retrievals and uncertainty analysis of aerosol single scattering albedo from MFRSR measurements, J. Quant. Spectrosc. Radiat. Transf., 150, 95–106, doi:10.1016/j.jqsrt.2014.08.012, 2015.